Eur. Phys. J. Special Topics **229**, 1545–1555 (2020)

https://doi.org/10.1140/epjst/e2020-900128-y

THE EUROPEAN PHYSICAL JOURNAL SPECIAL TOPICS

Regular Article

Effects of higher-order multipoles of the lunar disturbing potential on elongated orbits in cislunar space

Aaron J. Rosengren[1,a], Hossein Namazyfard[1], and Giorgio E. O. Giacaglia[2]

[1] Aerospace and Mechanical Engineering Dept., University of Arizona, Tucson, USA
[2] Mechanical Engineering Dept., University of Taubaté, Taubaté, SP, Brazil

Received 2 July 2019 / Received in final form 2 December 2019
Published online 29 May 2020

Abstract. For an Earth satellite in cislunar space, the effects of the third or higher-order harmonics in the solar disturbing function are negligible. For lunar perturbations, however, these terms become increasingly important as the semimajor axis increases. We investigate the effects of these higher-order multipole moments on circular, moderate, and highly elliptical orbits, where the semimajor axis is a relatively large fraction (∼20%) of the Moon's one. We specifically characterize the regions of cislunar space where the octupole-order approximation, often used in celestial and astrophysical dynamics for studying the stability and fates of hierarchical planetary systems, is actually a valid truncation of the gravitational interactions.

1 Introduction

The perturbing gravitational forces of the Moon and the Sun acting on Earth satellites cause both secular and periodic variations to the orbital elements [5,8,16,23,36]. For near-Earth satellites, the effects of these distant perturbing bodies are often negligible in comparison to that of the Earth's oblateness [6], but for satellite orbits that are very elongated or have semi-major axes of several Earth radii, these lunisolar gravitational perturbations can change the elements of the orbit to a measurable extent [2,5]. Mathematically, the problem can be cast as a perturbing potential that can be further expanded into a series of Legendre polynomials in the ratio of the radial distances, a small quantity for close satellite orbits [27]. Often, we can truncate the series to second order, so that the lunar and solar potentials are approximated with sufficient accuracy by quadrupole fields [2,17,23,27,35]. For a satellite in cislunar space, the effects of the third or higher-order harmonics in the solar disturbing function are negligible. For lunar perturbations, however, these terms become increasingly important as the semimajor axis increases [1,18,19,23].

In the celestial and astrophysical dynamics context, the quadrupole approximation in the secular (doubly-averaged) hierarchical restricted three-body problem gives rise to the Lidov-Kozai mechanism [10,23]; thought to play an important role in the formation and evolution of many astronomical systems [28,33]. At that order of series

[a] e-mail: ajrosengren@email.arizona.edu

truncation, the perturber's argument of periapsis does not appear and the particle's normal component of angular momentum is conserved, enabling the particle's orbit to periodically exchange its eccentricity with inclination. Ford et al. [11], Lee and Peale [20], Katz et al. [14], and Naoz et al. [29] found that qualitatively different behaviors can occur when the octupole moment of the Legendre expansion is accounted for in the secular equations. Orbits can reach extremely high eccentricities and undergo chaotic flips from prograde to retrograde orientation [21,24].

For the vast majority of these studies, only a few comparisons have been made with direct gravitational N-body integrations [13,20,22,24,25,38]. Lee and Peale [20] found that the octupole-level secular theory is highly accurate for coplanar, hierarchical, two-planet systems with semi-major axes ratios (a/a') less than about 0.1, and reasonably accurate for systems with a/a' as large as 1/3, in the absence of orbital resonances of the mean-motion type. The general domain of validity of either the secular quadrupole and octupole approximations, however, has hitherto not been established.

Returning to the circumterrestrial domain, for the investigation of the Earth's magnetosphere and the interplanetary space outside of it, satellites with orbits of high eccentricity, large semi-major axis, and multi-day period are often used. A basic question we will address here is whether the octupolar order of approximation can sufficiently describe the orbital evolution of such systems. In particular, Lidov [23] stated that the parallactic term (third harmonic or octupole moment) can cause the eccentricity to build up more rapidly if the orbit is sufficiently large; specifically, that the parallactic term becomes effective when the object is at a distance of about 10 Earth radii. Similar assertions were made by Musen [27], Allan and Cook [2], and Cook and Scott [9], but no analysis was conducted to determine the quantitative effects of higher-order multipoles of the lunar expansion on such distant orbits.

Here, we recover classical secular (i.e., orbit-averaged) equations of motion, written in terms of the non-singular Milankovitch vectorial elements, that govern the long-term evolution of orbits subject to lunisolar perturbations [1,27]. We systematically compare numerical simulations of the quadrupole-order and octupole-order equations, respectively, against precise integrations of the full non-averaged equations of motion [3]. We ignore here the short-period correction terms in properly specifying the initial conditions for each formulation [37]; but this omission for singly-averaged systems is not as serious as it might at first appear [25,30]. We consider semi-major axes in the range of $4–8 \times 10^4$ km, all prograde (equatorial) inclinations, and distinct values of eccentricities of 0, 0.4, and 0.8, respectively. This covers the geosynchronous region, but also a wide range of the cislunar phase space relevant to both historic and current scientific missions launched by the US (e.g., AMPTE, Chandra X-ray Observatory, several EXPLORER series satellites) and Europe (e.g., XMM-Newton, Cluster II). The limit in semi-major axis was chosen to avoid any low-order lunar mean-motion resonances, which would invalidate the secular equations of motion. Future work will focus on hexadecapole- and higher-order multipole secular equations (qq.v. [13,38]) for treating multi-day period orbits.

2 Problem formulation and averaging

Perturbation theory in celestial mechanics often gives rise to nearly integrable, multi-dimensional, nonlinear Hamiltonian systems [4,32]. The Kepler Hamiltonian that describes the orbits of a test particle about a central body of gravitational parameter μ is given by

$$\mathcal{H}_K = \frac{1}{2}v^2 - \frac{\mu}{r} = -\frac{\mu}{2a}, \tag{1}$$

where $r = |\boldsymbol{r}|$, $\boldsymbol{r}$ being the position vector measured from the center of the body, $v = |\boldsymbol{v}|$, $\boldsymbol{v} = \dot{\boldsymbol{r}}$, and a is the particle's semi-major axis. The integrals of motion are the Hamiltonian $\mathcal{H}_K$, and the specific angular momentum and eccentricity vectors

$$\boldsymbol{H} = \boldsymbol{r} \times \boldsymbol{v}, \qquad \boldsymbol{e} = \frac{1}{\mu}\boldsymbol{v} \times \boldsymbol{H} - \frac{\boldsymbol{r}}{r}. \tag{2}$$

These vectorial integrals are related to the orbit eccentricity by $e = |\boldsymbol{e}|$ and semi-major axis by $H^2 = \mu a(1 - e^2)$, where $H = |\boldsymbol{H}|$. Geometrically, $\boldsymbol{H}$ points perpendicular to the orbital plane and $\boldsymbol{e}$ points from the central body toward the orbit's pericenter.

A noteworthy feature of celestial mechanics is the use of a potential function, from which the components of the total perturbing force in the coordinate directions can be derived by partial differentiation. Taking the central mass as the center of our dynamical system, the disturbing function (negative potential) arising from an external body with gravitational parameter μ' is

$$\mathcal{R} = \mu' \left[\frac{1}{|\boldsymbol{r} - \boldsymbol{r}'|} - \frac{\boldsymbol{r} \cdot \boldsymbol{r}'}{r'^3} \right], \tag{3}$$

where $\boldsymbol{r}'$ is the position vector of the perturbing body relative to the central mass and $r' = |\boldsymbol{r}'|$. Assuming $r/r' \ll 1$, the third-body disturbing function can be represented as an infinite series of Legendre polynomials $P_{l,0}$, where the relevant perturbation terms begin at the quadrupole order as [27]

$$\begin{aligned} \mathcal{R} &= \frac{\mu'}{r'} \sum_{l=2}^{\infty} \left(\frac{r}{r'} \right)^l P_{l,0}(\cos\psi) \\ &= \frac{\mu'}{r'} \left[\frac{r^2}{r'^2} \left(-\frac{1}{2} + \frac{3}{2}\cos^2\psi \right) + \frac{r^3}{r'^3} \left(-\frac{3}{2}\cos\psi + \frac{5}{2}\cos^3\psi \right) + \cdots \right], \end{aligned} \tag{4}$$

for which $rr'\cos\psi = \boldsymbol{r} \cdot \boldsymbol{r}'$. The disturbing function can be further expanded in the form of a Fourier-Taylor series of periodic terms, whose arguments are combinations of the orbital phase and orientation angles of the particle and the perturbing body, and whose coefficients depend on the size and shape (semimajor axes and eccentricities) of their orbits and the inclinations [7,12,15,17]:

$$\begin{aligned} \mathcal{R} = \mu' \sum_{l=2}^{\infty} \sum_{m=0}^{l} \sum_{p=0}^{l} \sum_{h=0}^{l} \sum_{q=-\infty}^{\infty} \sum_{j=-\infty}^{\infty} \frac{a^l}{a'^{l+1}} \epsilon_m \frac{(l-m)!}{(l+m)!} F_{l,m,p}(i) F_{l,m,h}(i') H_{l,p,q}(e) G_{l,h,j}(e') \\ \times \cos\left[(l-2p)\omega + (l-2p+q)M - (l-2h)\omega' - (l-2h+j)M' + m(\Omega - \Omega') \right], \end{aligned} \tag{5}$$

where a, e, i, Ω, ω, M are the particle's Keplerian orbital elements, the primed quantities refer to that of the perturbing body, the functions $H_{l,p,q}(e)$ and $G_{l,h,j}(e')$ are polynomials of order $e^{|q|}$ and $e'^{|j|}$, respectively, and the functions F are polynomials in the sine and cosine of half the respective inclinations. This expansion gives rise to the notion of separation of perturbing effects into periodic and secular variations and the distinction between fast and slow time variables [26]. The orbit-averaging technique effectively involves discarding all terms that depend on the fast-varying mean anomalies; i.e., setting successively $l - 2p + q = 0$ (single averaging) and $l - 2h + j = 0$ (double averaging). Purely secular perturbations are related to terms in the disturbing function expansion with $l - 2p = 0$, $l - 2p + q = 0$, $l - 2h = 0$, $l - 2h + j = 0$, and $m = 0$; these can occur only for even powers of l. Thus, only in the case of an orbital resonance (a harmonic angle librating), should one generally expect the odd powers to contribute to the long-term dynamics.

The Hamiltonian governing the perturbed motion of the test partial can be written as

$$\mathcal{H} = \mathcal{H}_K - \mathcal{R}. \tag{6}$$

The perturbation equations can be written in terms of action-angle variables (canonical form) or really any complete set of functionally-independent integrals of the unperturbed system [4]. Qualitatively, the perturbed Keplerian orbit gains two additional frequencies, consisting of a precession of the orbit plane and a rotation of the major axis in the moving orbit plane (nodal and apsidal motion), which are slow relative to the orbital frequency (i.e., the mean motion). If there are no commensurability relationships involving the mean motions, the Hamiltonian can be averaged over the successive orbital phases (mean anomalies) of the system to obtain the secular equations of motion that approximately govern the long-term behavior.

Averaging can be carried out systematically for each term in the third-body multipole expansion [q.v., 32]. The singly-averaged equation of motion to quadrupole order (2nd order in r/r') can be written in the form [1,27]

$$\dot{\boldsymbol{h}}_{\rm quad} = \frac{3\mu'}{2nr'^5}\Big[5\left(\boldsymbol{e}\cdot\boldsymbol{r}'\right)\boldsymbol{e}\times\boldsymbol{r}' - \left(\boldsymbol{h}\cdot\boldsymbol{r}'\right)\boldsymbol{h}\times\boldsymbol{r}'\Big], \tag{7}$$

$$\dot{\boldsymbol{e}}_{\rm quad} = \frac{3\mu'}{2nr'^5}\Big[5\left(\boldsymbol{e}\cdot\boldsymbol{r}'\right)\boldsymbol{h}\times\boldsymbol{r}' - \left(\boldsymbol{h}\cdot\boldsymbol{r}'\right)\boldsymbol{e}\times\boldsymbol{r}' - 2r'^2\boldsymbol{h}\times\boldsymbol{e}\Big]. \tag{8}$$

Here $n^2 = \mu/a^3$, $\boldsymbol{h} = \boldsymbol{H}/na^2$, and we note that the particle's semi-major axis a is constant on average and that solutions are restricted by the constraints $\boldsymbol{h}\cdot\boldsymbol{e} = 0$ and $\boldsymbol{h}\cdot\boldsymbol{h} + \boldsymbol{e}\cdot\boldsymbol{e} = 1$. The scaled angular momentum vector and eccentricity vector, while not canonical variables, have decided advantages over classical element sets in formulating the perturbation equations [13,14,25,35].

The singly-averaged equations resulting from the octupole term can be stated as [1]

$$\dot{\boldsymbol{h}}_{\rm oct} = -\frac{15a\mu'}{16nr'^7}\Big\{\Big[35(\boldsymbol{e}\cdot\boldsymbol{r}')^2 - 5(\boldsymbol{h}\cdot\boldsymbol{r}')^2 + r'^2(1-8e^2)\Big]\boldsymbol{e}\times\boldsymbol{r}' - 10(\boldsymbol{e}\cdot\boldsymbol{r}')(\boldsymbol{h}\cdot\boldsymbol{r}')\boldsymbol{h}\times\boldsymbol{r}'\Big\} \tag{9}$$

$$\dot{\boldsymbol{e}}_{\rm oct} = -\frac{15a\mu'}{16nr'^7}\Big[\Big\{\Big[35(\boldsymbol{e}\cdot\boldsymbol{r}')^2 - 5(\boldsymbol{h}\cdot\boldsymbol{r}')^2 + r'^2(1-8e^2)\Big]\boldsymbol{h}\times\boldsymbol{r}' - 10(\boldsymbol{e}\cdot\boldsymbol{r}')(\boldsymbol{h}\cdot\boldsymbol{r}')\boldsymbol{e}\times\boldsymbol{r}'\Big\} - 16r'^3(\boldsymbol{e}\cdot\boldsymbol{r}')\boldsymbol{h}\times\boldsymbol{e}\Big]. \tag{10}$$

For a satellite on an initially circular orbit ($\boldsymbol{e} = 0$), the orbit remains circular throughout under the quadrupole order (or other even degree Legendre polynomials); but this particular solution is destroyed when the effects of $l = 3$ (or other odd degree Legendre polynomials) are taken into account. So even degree polynomials are more relevant in the long-term dynamics, but the octupolar order is definitely needed when discussing the perturbed dynamics of low-eccentricity orbits.

Note that both the quadrupole-order and octupole-order equations can subsequently be averaged over the perturber's motion [14,29]; however, these will not be used here.

3 Numerical exploration

It is the mechanical structure of the satellites and the nature of its orbit that determine which perturbing forces are significant and which are negligible for any

particular application. We are not interested here in precise solutions for specific initial conditions, but rather in quantifying the errors produced by series truncation and averaging of gravitational force potentials. As such, our perturbation model is limited to lunar and solar gravity, and we use the `THALASSA` software tool[1] [3] to produce highly accurate trajectories under the restricted 4-body problem (Earth-Satellite-Moon-Sun) for an expansive grid of initial conditions. We specifically consider semi-major axes in the range of $4\text{–}8 \times 10^4$ km, all prograde (equatorial) inclinations, and distinct values of eccentricities of 0, 0.4, and 0.8, respectively. Simulations are carried out for 100 years ($\sim 10^4$ orbital revolutions), and the results are displayed in a series of "error" maps, where the colorbar corresponds to the root mean square (RMS) of the difference between the `THALASSA` "truth" trajectory and that produced from the various approximate models. In particular, we compute the RMS of the difference in the Delaunay action $\mathscr{H}$, which is conjugate to the ascending node:

$$\mathscr{H} = \sqrt{\mu a(1-e^2)}\cos i. \tag{11}$$

The units of length and time are normalized so that the geostationary distance is unity and the period of Earth's rotation is equal to 2π; consequently, $\mu = 1$. (As an example, for circular equatorial orbits of semi-major axis 40 000 km and 80 000 km, respectively, $\mathscr{H} \approx 0.9740$ and $\mathscr{H} \approx 1.3774$. In the simulations considered, $\mathscr{H} \in [0, 1.3774]$, initially.)

Figure 1 shows the results of this error analysis corresponding to six different initial values of semi-major axis, inclination, and eccentricity. The J2000 epoch date was used for all simulations, and the initial angular quantities were set to $(\Omega, \omega, M) = (180°, 90°, 0)$. Note that other specific combinations of angles would lead to different evolutions, in general, particularly when subjected to a resonance effect. We ignore here the short-period correction terms (i.e., the osculating-to-mean element transformation; see, e.g., [30]) and thus the initial conditions are the same for each formulation. The positions of both the Moon and Sun were computed using the JPL ephemeris (DE431). It can be seen from Figure 1 that the octupole approximation must be considered when analyzing quasi-circular orbits, and that higher-order multipoles are needed for more distant orbits.

An output time step of 10 days was used in all simulations and the RMS error in normalized Delaunay $\mathscr{H}$ can be computed. For the example evolutions of Figure 1, this varied between 0.0017 and 0.2755 for the secular quadrupole model and between 0.0017 and 0.0730 for the octupole-level dynamics. Figure 2 shows error maps corresponding to three different initial eccentricities for 200×200 grids of initial (equatorial) inclinations and semi-major axes. Each grid point, together with $(\Omega, \omega, M) = (180°, 90°, 0)$, was used to form the full orbital element state vector, and the $l = 2$ and $l = 3$ singly-averaged equations, respectively, were propagated for at most 100 years and compared against direct gravitational N-body integrations (i.e., no truncations or averaging).

We are not concerned here with the nature of the structures visible in each map, and, generally speaking, the results would be more sensible if casted in ecliptic inclinations as opposed to equatorial values. The Moon's inclination to the Earth's equator varies between roughly 18.3° and 28.6°, on account of the gravitational

[1] The `THALASSA` Earth-satellite orbit propagation tool, which is freely available through a GitLab repository (URL: https://gitlab.com/souvlaki/thalassa), uses the variable step-size and order (up to 12th) `LSODAR` solver to numerically integrate a collection of regularized formulations of the full equations of motion, which automatically selects the solution algorithm between the implicit Adams-Bashforth-Moulton and backwards differentiation formulas.

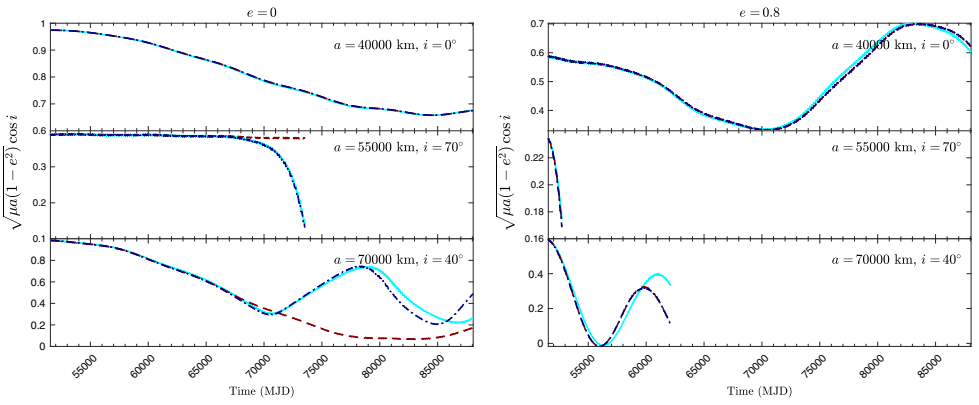

Fig. 1. Evolution of the Delaunay $\mathscr{H}$ for distant circumterrestrial orbits of eccentricity 0 (*left*) and 0.8 (*right*). The J2000 epoch date was used for all simulations, and the initial node, perigee, and mean anomaly angles were set to $(\Omega, \omega, M) = (180°, 90°, 0)$. Each (a, i) pair was used to form the full orbital element state vector, and the quadrupole-order (*red, dashed*) and octupole-order (*blue, dash-dot*) averaged equations were propagated for at most 100 years and compared against direct N-body integrations using `THALASSA` (*cyan*). In the case of an Earth re-entry trajectory, the evolutions were only compared over the shortest orbital lifetime, according to all dynamical models. Here, $\mathscr{H}$ is dimensionless and the time unit is the modified Julian date.

action of the Sun. The results appear to be in agreement with the findings of Lee and Peale [20] for small semi-major axis ratios; the range of validity, however, shrinks for specific non-coplanar, hierarchical systems. The secular octupole-order equations give significant improvements over that at quadrupolar order for the maps produced with initially circular orbits (Fig. 2, top panel). However, no improvements are gained from this additional Legendre term when considering higher initial eccentricities (middle and bottom panels), where the initial orbit apogees can exceed 15 Earth radii. (Note that the larger RMS values along the zero degrees equatorial inclination at distinct semi-major axis values, appearing in the top panel only, are an artifact; as these points are of no dynamical significance for the lunisolar perturbation problem and no formulation treated herein suffers from any singularities.)

The two approximations made in forming the secular equations are a truncation of the infinite series expansion and an averaging (at the first order) of the Hamiltonian over the satellite's orbital motion. While higher-order averaging techniques can in principle produce more accurate results [4], the fundamental limitation in recovering the N-body trajectories is the truncation order. Figure 3 shows a comparison between the quadrupole-order singly-averaged and non-averaged error maps for initially circular orbits. The latter map was made with the solar potential truncated at quadrupolar order (a valid assumption for all of circumterrestrial space) and the lunar potential also truncated at the $l = 2$ term (Eq. (4)), using `THALASSA`. The same structures are present in each map, but within their boundaries, averaging leads to larger RMS values. Figure 4 shows the comparison at octupole-order for an initial eccentricity of 0.4. In this case, for these more distant orbits, the averaged and non-averaged maps are in better agreement as the errors here are dominated by the truncation order.

From a harmonic analysis of the perturbations (Eq. (5)), one can generally conclude that a truncation should always be performed at an even degree Legendre polynomial [19]. Figure 5 shows maps made with the solar potential truncated at

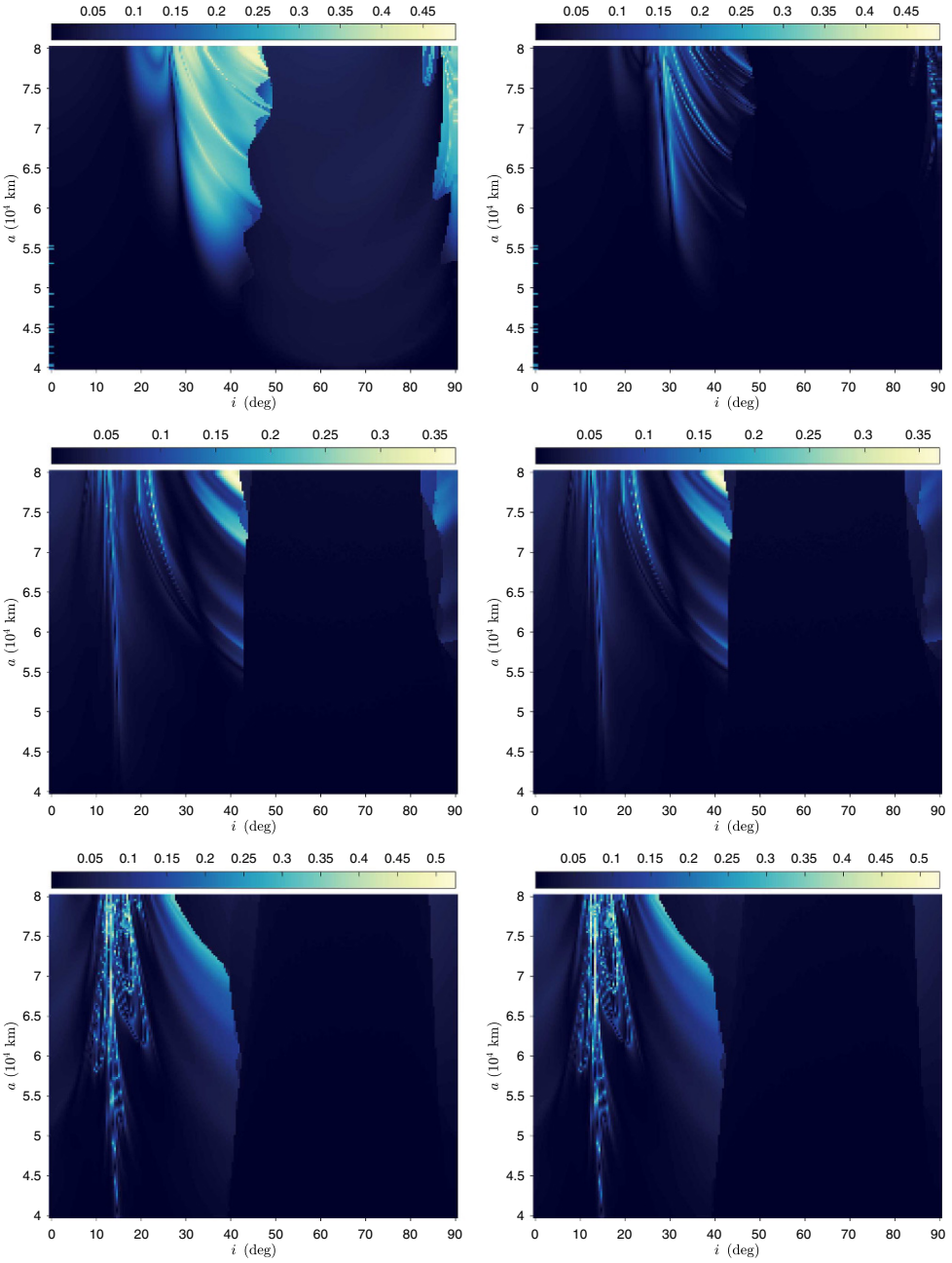

Fig. 2. Error maps in the (equatorial) inclination–semi-major axis phase space for initial eccentricities of 0 (*top*), 0.4 (*middle*), and 0.8 (*bottom*). The J2000 epoch date was used for all simulations, and the initial node, perigee, and mean anomaly angles were set to $(\Omega, \omega, M) = (180°, 90°, 0)$. Each grid point was used to form the full orbital element state vector, and the quadrupole-order (*left*) and octupole-order (*right*) averaged equations were propagated for 100 years and compared against direct gravitational N-body integrations using `THALASSA`. The colorbar indicates the root mean square of the difference in Delaunay action $\mathscr{H}$, as obtained from numerical integrations of the various dynamical models.

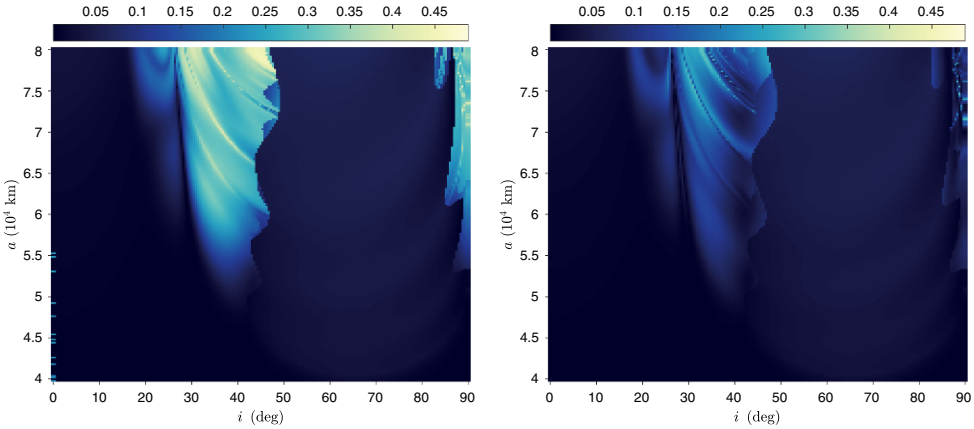

Fig. 3. Error maps in the (equatorial) inclination–semi-major axis phase space for an initial eccentricity of 0. The J2000 epoch date was used for all simulations, and the initial node, perigee, and mean anomaly angles were set to $(\Omega, \omega, M) = (180°, 90°, 0)$. Each grid point was used to form the full orbital element state vector, and the $l = 2$ singly-averaged (*left*) and $l = 2$ truncated, non-averaged (*right*) equations, respectively, were propagated for 100 years and compared against direct gravitational N-body integrations (i.e., no truncations). The colorbar indicates the root mean square of the difference in Delaunay action $\mathscr{H}$, as obtained from numerical integrations of the various dynamical models.

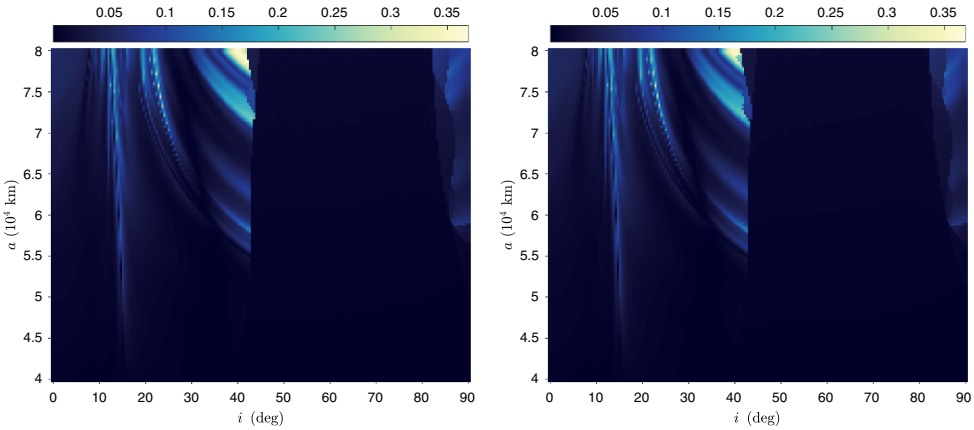

Fig. 4. Error maps in the (equatorial) inclination–semi-major axis phase space for an initial eccentricity of 0.4. The J2000 epoch date was used for all simulations, and the initial node, perigee, and mean anomaly angles were set to $(\Omega, \omega, M) = (180°, 90°, 0)$. Each grid point was used to form the full orbital element state vector, and the $l = 3$ singly-averaged (*left*) and $l = 3$ truncated, non-averaged (*right*) equations, respectively, were propagated for 100 years and compared against direct gravitational N-body integrations (i.e., no truncations). The colorbar indicates the root mean square of the difference in Delaunay action $\mathscr{H}$, as obtained from numerical integrations of the various dynamical models.

the $l = 2$ term and the lunar potential truncated at the $l = 4$ and $l = 6$ (Eq. (4)), respectively, using `THALASSA`. We can see that already at hexadecapole-order, the discrepancy with the N-body integrations nearly vanishes.

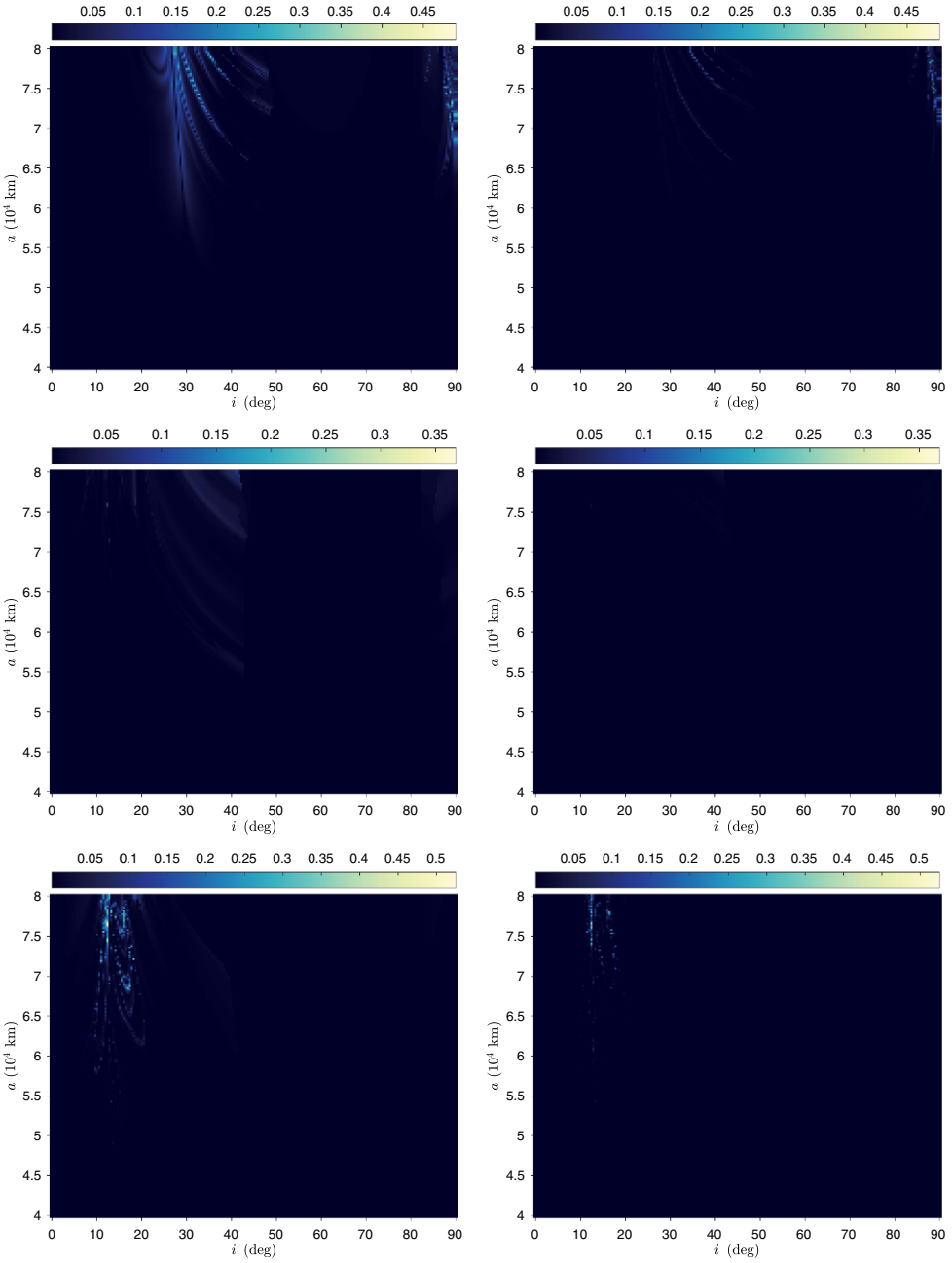

Fig. 5. Error maps in the (equatorial) inclination–semi-major axis phase space for initial eccentricities of 0 (*top*), 0.4 (*middle*), and 0.8 (*bottom*). The J2000 epoch date was used for all simulations, and the initial node, perigee, and mean anomaly angles were set to $(\Omega, \omega, M) = (180°, 90°, 0)$. Each grid point was used to form the full orbital element state vector, and the $l = 4$ (hexadecapole; *left*) and $l = 6$ (*right*) truncated, non-averaged equations were propagated for 100 years and compared against direct gravitational N-body integrations, all using `THALASSA`. The colorbar indicates the root mean square of the difference in Delaunay action $\mathscr{H}$, as obtained from numerical integrations of the various dynamical models.

4 Discussion and conclusions

Averaging appears to be such a natural procedure that many dynamicists do not even bother to justify the process [26]. Though averaging has proven its use over the past five decades, its validity should be constantly tested against precise simulations of the full system; especially considering the ubiquity of orbital resonances in celestial mechanics (see, e.g., [31]). Herein, we have compared detailed numerical simulations of singly-averaged and non-averaged systems, with a focus on the octupole-order multipole of the third-body gravitational potential. For semi-major axes ratios of 0.21 or less, as considered herein, only in the initially circular orbit case does the octupole-level singly-averaged theory lead to notable improvements over the quadrupolar order, at least for the Earth-Moon-Sun system. For deeper space probes, the secular equations must be developed at the hexadecapole-order, or higher. The implications for the stability and fates of hierarchical planetary systems remain an open question. The doubly-averaged equations used in these celestial dynamics applications must still be systematically vetted against the full system, where it becomes more important to properly account for the short-periodic corrections in the initial conditions. Future work should address these questions, as well as consider orbits where the semi-major axis is a substantial fraction of the Moon's (e.g., the Soviet space probe, Luna 3 (1959 Theta 1) or the recently launched, Transiting Exoplanet Survey Satellite (TESS; 2018-038A)), where lunar mean-motion resonances must be considered.

Some results of this paper were presented at the XIX Colóquio Brasileiro de Dinâmica Orbital, CBDO, 2018, São José dos Campos, SP, Brazil. This paper has benefited from insightful comments made by D. Amato, I. Gkolias, and M. Lara. This research has made use of the THALASSA software package (Astrophysics Source Code Library, record ascl:1905.018) and NASA's Astrophysics Data System.

References

1. R.R. Allan, Q. J. Mech. Appl. Math. **15**, 283 (1962)
2. R.R. Allan, G.E. Cook, Proc. R. Soc. Lond. A **280**, 97 (1964)
3. D. Amato, C. Bombardelli, G. Baú, V. Morand, A.J. Rosengren, Celest. Mech. Dyn. Astron. **131**, 21 (2019)
4. A. Morbidelli, *Modern celestial mechanics: aspects of solar system dynamics* (Taylor & Francis, London, 2002)
5. L. Blitzer, Am. J. Phys. **27**, 634 (1959)
6. D. Brouwer, Astron. J. **64**, 378 (1959)
7. A. Celletti, C. Galeş, G. Pucacco, A.J. Rosengren, Celest. Mech. Dyn. Astron. **112711**, 259 (2017)
8. G.E. Cook, Geophys. J. **6**, 271 (1962)
9. G.E. Cook, D.W. Scott, Planet. Space Sci. **15**, 1549 (1967)
10. A.C.M. Correia, J. Laskar, F. Farago, G. Boué, Celest. Mech. Dyn. Astron. **111**, 105 (2011)
11. E.B. Ford, B. Kozinsky, F.A. Rasio, Astrophys. J. **535**, 385 (2000)
12. G.E.O. Giacaglia, Celest. Mech. **9**, 239 (1974)
13. A.S. Hamers, H.B. Perets, F. Antonini, S.F. Portegies Zwart, Mon. Not. R. Astron. Soc. **449**, 4221 (2015)
14. B. Katz, S. Dong, R. Malhotra, Phys. Rev. Lett. **107**, 181101 (2011)

15. W.M. Kaula, Astron. J. **67**, 300 (1962)
16. Y. Kozai, SAO Spec. Rep. **22**, 7 (1959)
17. M.T. Lane, Celest. Mech. Dyn. Astron. **46**, 287 (1989)
18. M. Lara, J.F. San-Juan, L.M. López, P.J. Cefola, Celest. Mech. Dyn. Astron. **113**, 435 (2012)
19. M. Lara, J.F. San-Juan, D. Hautesserres, CEAS Space J. **10**, 3 (2018)
20. M.H. Lee, S.J. Peale, Astrophys. J. **592**, 1201 (2003)
21. G. Li, S. Naoz, M. Holman, A. Loeb, Astrophys. J. **791**, 86 (2014)
22. G. Li, S. Naoz, M. Holman, A. Loeb, Astrophys. J. **785**, 116 (2014)
23. M.L. Lidov, Planet. Space Sci. **9**, 719 (1962)
24. Y. Lithwick, S. Naoz, Astrophys. J. **742**, 94 (2011)
25. L. Luo, B. Katz, S. Dong, Mon. Not. R. Astron. Soc. **458**, 3060 (2016)
26. R.A. Mardling, Mon. Not. R. Astron. Soc. **435**, 2187 (2013)
27. P. Musen, J. Geophys. Res. **66**, 2797 (1961)
28. S. Naoz, Annu. Rev. Astron. Astrophys. **54** 441 (2016)
29. S. Naoz, W.M. Farr, Y. Lithwick, F.A. Rasio, J. Teyssandier, Nature **473**, 187 (2011)
30. T. Nie, P. Gurfil, S. Zhang, Celest. Mech. Dyn. Astron. **131**, 29 (2019)
31. A.J. Rosengren, D.K. Skoulidou, K. Tsiganis, G. Voyatzis, Adv. Space Res. **63**, 443 (2019)
32. D.J. Scheeres, *Orbital motion in strongly perturbed environments: applications to asteroid, comet and planetary satellite orbiters* (Springer-Praxis, Berlin, 2012)
33. I.I. Shevchenko, *The Lidov-Kozai effect – applications in exoplanet research and dynamical astronomy* (Springer, Berlin, 2017)
34. V.V. Sidorenko, Celest. Mech. Dyn. Astron. **130**, 4 (2018)
35. S. Tremaine, T.D. Yavetz, Am. J. Phys. **82**, 769 (2014)
36. E. Upton, A. Bailie, P. Musen, Science **130**, 1710 (1959)
37. H.G. Walter, Astron. J. **72**, 994 (1967)
38. C.M. Will, Phys. Rev. A **96**, 023017 (2017)